Express Polymer Letters Vol.16, No.9 (2022) 978–995
Available online at www.expresspolymlett.com
https://doi.org/10.3144/expresspolymlett.2022.71

Research article

Multifunctional properties of chemically reduced graphene oxide and silicone rubber composite: Facile synthesis and application as soft composites for piezoelectric energy harvesting

Vineet Kumar[1], *Tapas Kumar Mandal*[1], *Anuj Kumar*[2], *Md Najib Alam*[1], *Nargish Parvin*[1], *Sang Woo Joo*[1], *Dong Joo Lee*[1], *Sang-Shin Park*[1*]

[1]School of Mechanical Engineering, Yeungnam University, 280 Daehak-ro, 38541 Gyeongsan, South Korea
[2]School of Chemical Engineering, Yeungnam University, 280 Daehak-ro, 38541 Gyeongsan, South Korea

Received 2 March 2022; accepted in revised form 15 May 2022

Abstract. The 6th element of the periodic table is undoubtedly one of the most incredible aspects of creation. Graphene has a 2-D sheet structure comprised of strong covalent bonds between sp^2 hybridized carbon atoms and has attracted much research interest because of its unique physicochemical properties. However, the controlled syntheses of mono-layered and few-layered graphene remain topics of research concern. In the present work, chemically reduced graphene oxide (CRGO) was synthesized by 'top-down' using the modified Hummers' method. CRGO and room-temperature-vulcanized silicone rubber (RTV-SR) were mixed to prepare composites with different CRGO loadings. We found that as little as 2 per hundred parts of rubber [phr] CRGO in RTV-SR transformed the normally rigid RTV-SR into a soft composite with a hardness decrease to 15. Moreover, the compressive modulus falls to 0.6 MPa. However, the dissipation losses decrease at 2 phr CRGO, which is a good property. For tensile mechanical properties, the fracture strain increases to 100% while tensile strength falls sharply to 0.1 MPa. Moreover, the electrical conductivity increases as the amount of CRGO increases. So, composite with soft nature and higher electrical properties are useful for various applications such as soft robotics or soft piezoelectric energy harvesting. In this work, the piezoelectric energy harvesting was performed by monitoring the output voltages generated. Output voltages were stable for RTV-SR but increased with increasing cycle number for RTV-SR/CRGO-based composites. This study provides insights into the use of soft RTV-SR/CRGO composites for soft robotics, actuation, energy harvesting, and vehicle applications.

Keywords: *polymer composites, reinforcements, mechanical properties, chemically reduced graphene oxide, silicone rubber*

1. Introduction

The preparation and characterization of composites based on silicone rubber (SR) containing nanofillers such as carbon nanotube (CNT) [1], graphene (GE) [2], or carbon black (CB) [3] has absorbed considerable research effort during the last 2–3 decades. SR has poor electrical conductivity, mechanical properties, thermal conductivity, and barrier properties [4], and nanofillers have been added to improve its properties [1–3, 5]. Some authors have shown that the incorporation of CNT at 2 phr loading improves the Young's modulus of SR by 272% and significantly enhances its electrical properties [6]. Several methods have been used to improve the properties of polymer composites, such as (a) the incorporation of functionalized fillers, (b) the use of hybrid fillers, and (c) the use of polymer blends [7].

Graphene oxide (GO) is a 2D (two-dimensional) flake material that can be obtained by oxidizing graphene and functionalized with different groups (*e.g.*, car-

*Corresponding author, e-mail: pss@ynu.ac.kr

boxyl, epoxy, and others). CRGO can be prepared by treating graphene with acids and different types of oxidizing agents and subsequently reducing it chemically. CRGO also has several novel properties, which include excellent stress transfer and higher properties [8]. Further investigations are reported on CRGO reinforced polymer composites that show temperature-dependent creep and recovery behavior [8]. The experiments demonstrate that the incorporation of CRGO in polystyrene polymer matrix improves the thermal and mechanical properties significantly [9]. Studies show that CRGO and their derivatives, such as multi-dimensional graphene structures act as a superior source of high-performance composites and are useful for various applications such as nano-generators for energy harvesting and coatings [10–13]. Studies are reported that demonstrate the use of CRGO ideally to obtain balanced electrical, mechanical, and thermal properties in an epoxy matrix [14].

Many polymer types, such as thermoplastics, thermosets, and elastomers, have been used as matrices for CRGO-containing composites, though elastomers are more often used because of their wide applications [15]. Silicone rubber (SR) is a type of elastomer composed of silicon, carbon, hydrogen, and oxygen [16], and typically, SRs have high fracture strengths and excellent chemical stabilities and electrical insulating properties [16]. These characteristics of SRs have resulted in their widespread use in automotive, flexible electronics, and medical implant end uses [16]. SRs may be classified based on the vulcanization methods used, that is, as room temperature vulcanized (RTV), low temperature vulcanized (LTV), or high temperature vulcanized (HTV) SRs, though the majority of studies have been conducted using RTV-SRs because they are easily processed, cured, and have low viscosities.

Various studies have investigated the use of graphene, few-layered graphenes, or multilayered graphenes in elastomeric matrices [17, 18]. Most have focused on CRGO reinforced polymer matrices [19], but a few have investigated the characteristics of RTV-SR/CRGO composites. In this work, CRGO flake with different surface functionalities was used as nano-fillers in RTV-SR matrices. The studies on CRGO-filled silicone rubber, and its energy harvesting properties are not understood well still, and this work provides an overview on this aspect. Moreover, the use of CRGO was found to be effective in making the composites ultra-soft and highly flexible as targeted. Such as, by introducing 2 phr of CRGO, the hardness falls from 28 (unfilled) to 15. Our motivation in the present study is to explore robust and ultra-soft piezoelectric energy harvesting devices with high flexibility and high durability to be useful for industrial use. Here, we describe a simple way to harvest energy through composites based on virgin and CRGO-based substrate and CNT-based electrode. Moreover, efficient filler networks of CRGO were demonstrated via improved electrochemical properties, and a decrease in cross-linking density leads to the formation of mechanically soft composites with high fracture strain which are suitable for soft applications, but their behavior is not understood fully. Besides this, this work attention the readers to a possible correlation between mechanical properties with change in cross-linking density, pH of CRGO, and efficient filler networking and filler dispersion in enhancing electrical properties. These properties were helpful in obtaining high voltage via a piezoelectric energy harvesting device.

Summary of the literature survey and novelty of present work over existing work (Table 1).

2. Experimental

2.1. Materials

RTV-SR silicone rubber (KE441, Shin-Etsu, Japan) was used as the elastomer matrix for preparing CRGO-based composites. CAT-RM (Shin-Etsu, Japan) was

Table 1. Literature review on existing work and this work.

Sample No.	Polymer	Filler	Property	Applications	Reference
1	Poly(methyl methacrylate)	CRGO	Mechanical properties	Not studied	[8]
2	Polystyrene	CRGO	Mechanical and thermal properties	Not studied	[9]
3	–	Multi-dimensional graphene	Mechanical, thermal and electrical properties	Not studied	[10]
4	Epoxy	CRGO	Mechanical, thermal and electrical properties	Not studied	[14]
5	Silicone rubber	CRGO	Mechanical and electrical properties	Piezoelectric energy harvesting	This work

used as the vulcanizing agent. This vulcanizing agent is a two-component liquid rubber (for mold making) contained by propyleneglycolnonomerhylerhemcelae (PGMEA) and cyclopentanone. PGMEA is solvent. We found that a catalyst is used for vulcanization, and its details are not provided by the company. But it is a condensation reaction catalyst as provided by the supplier. Graphite nanoplatelets (97% pure, GNP, BET surface area of >420 m^2/g; purchased from Asbury Mills, Asbury, USA) were used to prepare CRGO. Potassium permanganate ($KMnO_4$; purity 99%) was purchased from Neo Froxx (LC-7081), and phosphoric acid (85% pure, H_3PO_4), sulphuric acid (97% pure, H_2SO_4), and hydrogen peroxide (35% pure, H_2O_2) were obtained from Merck, Korea. The mold-release agent was purchased from Nabakem, Korea.

2.2. Preparation of CRGO from GNP

The CRGO was prepared by oxidizing GNP powder using Hummers' modified method [20] and then reduced chemically. Hummers' method was modified by removing the $NaNO_3$ and adding H_3PO_4. Initially, 30 g of GNP was added to concentrated H_2SO_4 (1000 ml) under continuous stirring in an ice bath for 1 h, and then 100 ml of H_3PO_4 was added and stirred for 2 h. $KMnO_4$ (100 g) was then added and stirred for 1 h and then sonicated for 2 h (all on ice). The reaction system was then transferred to a 60 °C oil bath and vigorously stirred for about 0.5 h, 1500 ml water was added, and the solution was stirred for 30 mins at 95 °C. Slow addition of H_2O_2 (30%, 50 ml) with stirring for 1 h turned the color of the solution from dark brown to yellow. The mixture was then filtered and washed with 1:10 HCl aqueous solution to remove metal ions and centrifuged (8000 rpm for 3×6 min) and then washed three times with 100% ethanol and three times with DI water. The resulting CRGO powder was dried in air at 100 °C for 24 h and suspended in 70% ethanol (0.6 g/ml) for further use.

2.3. Preparation of CRGO and CRGO/RTV-SR composites

The preparation of the RTV-SR/CRGO composites was initiated by spraying a mold with a mold release agent and leaving it to dry for 3 h. Liquid RTV-SR solution (100 phr) was placed in a container and 0.5, 1, or 2 phr of CRGO (Table 2) was added and mixed for 10 minutes when a vulcanizing agent was added at 2 phr and mixed for ~1 min. The mixture was then poured into the mold, pressed manually, and then left for 24 h to cure. Finally, composites were removed from the mold for testing. A schematic of the process is shown in Figure 1.

2.4. Characterization techniques

2.4.1. FESEM microscopy of CRGO powder

The surface and morphology of CRGO powder were studied by a field emission SEM (S-4100, Tokyo, Japan). Elemental mapping of CRGO powder was performed by EDX. CRGO powder was ion-sputtered with platinum for 2 mins before FESEM to improve surface conductivity.

2.4.2. TEM microscopy of CRGO powder

CRGO powder morphology was investigated by high-resolution TEM (FEI Tecnai G2 F20 TEM HRTEM). Briefly, TEM samples were prepared by placing a drop of CRGO solution in ethanol onto a non-coated copper grid and allowing the solvent to evaporate in the air at room temperature. HRTEM images were recorded using a Gatan K2 Summit direct-detection electron-counting camera at an operating voltage of 300 kV.

2.4.3. XRD analysis of CRGO powder

XRD was performed on CRGO powder using a PANalytical X'PertPRO MPD unit at an operating voltage of 40 kV and 30 mA using Cu K_α as the X-ray source (λ = 1.540598 Å) over a 2θ angle range of 5–80° at a scan rate of 10°/min.

2.4.4. Raman spectra of CRGO powder

Raman spectra of CRGO powder were obtained using a XploRA™ PLUS unit (Horiba Instruments, Japan) at a laser wavelength of 532 nm. Raman spectra are usually used to determine the structural properties of CRGO flakes (*e.g.*, defect densities, structural defects, and a number of graphene layers stacked).

2.4.5. FTIR spectra of CRGO powder and RTV-SR/CRGO nanocomposites

FT-IR spectroscopy of CRGO powder and RTV-SR/CRGO nanocomposites was carried out on a Perkin-Elmer FTIR spectrometer in transmittance mode over the wavenumber range 400–4000 cm^{-1}.

2.4.6. XPS spectra of CRGO powder

XPS analysis (ESCALAB 250) using a monochromatic Al K_σ X-ray source ($h\nu$ = 1486.6 eV; spot size

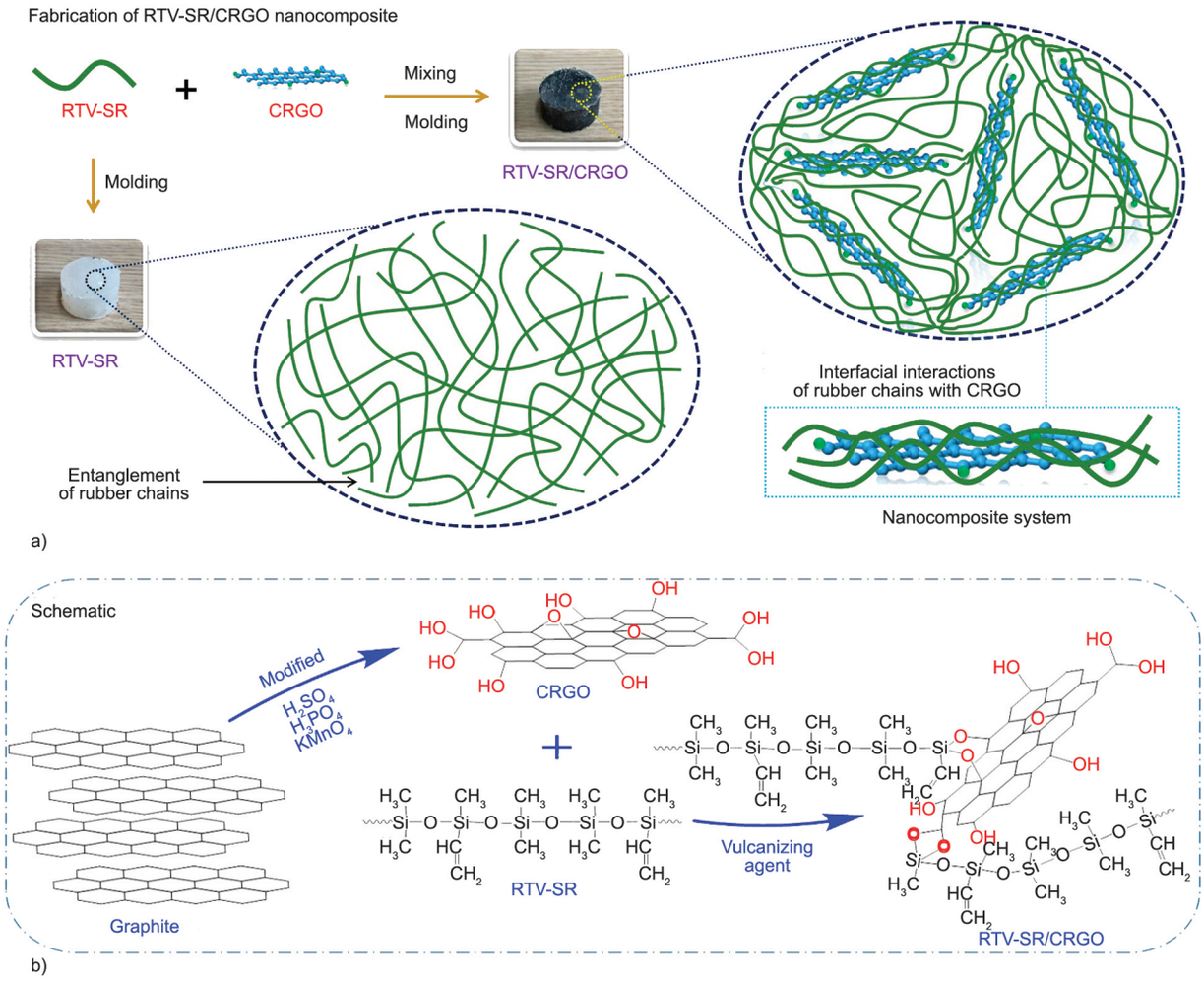

Figure 1. Preparation, fabrication (a), and schematic representation of RTV-SR/CRGO composites (b).

Table 2. Filler loadings in the RTV-SR composites.

Formulation	RTV-SR [phr]	CRGO [phr]			Vulcanizing agent [phr]
RTV-SR/CRGO	100	0.5	1	2	2

200 μm) was used to estimate binding energies and interactions in CRGO powder.

2.4.7. Cross-linking density and thermodynamics of RTV-SR/CRGO nanocomposites

Thermodynamic parameters such as Gibbs free energy (ΔG) and conformational entropy (ΔS) was calculated based on Flory–Huggins equation [21] (Equation (1)):

$$\Delta G = RT\left[\ln(1-V_r) + V_r + \chi V_r^2\right] \quad (1)$$

where R is the universal gas constant, T is the temperature in absolute scale (298 K), and V_r is the volume fraction of rubber in the swollen specimen. The volume fraction of rubber was calculated by equilibrium swelling the rubber sample in toluene for 7 days. The V_r was calculated as Equation (2):

$$V_r = \frac{\frac{w_r}{d_r}}{\frac{w_r}{d_r} + \frac{w_s}{d_s}} \quad (2)$$

where w_r and w_s are the weight of rubber and solvent, respectively and dr and ds are the densities of rubber and solvent, respectively.

The ΔS values were calculated based on Equation (3) considering no internal energy change during swelling [22]:

$$\Delta G = -T\Delta S \quad (3)$$

The cross-link densities were measured based on Flory–Rehner equation [23] as Equation (4):

$$V_c = -\frac{\ln(1-V_r) + V_r + \chi V_r^2}{V_s d_r\left(V_r^{1/3} - \frac{V_r}{2}\right)} \quad (4)$$

where V_c is the cross-link density, $\chi = 0.465$ is the interaction parameter between silicone rubber and toluene [24] (solvent), $V_s = 106.2$ is the molar volume of toluene, and the remaining parameters are the same as above.

2.4.8. Mechanical properties of RTV-SR/CRGO nanocomposites

Compressive and tensile mechanical properties of nanocomposites were determined using a universal testing machine (UTM, Lloyd Instruments, West Sussex, UK). Compressive properties were estimated using cylindrical samples (20 mm diameter and 10 mm thick) at a strain rate of 2 mm/min at max. strain up to 35%. Properties such as compressive moduli and compressive stress-strains were determined from compressive test results. The tensile mechanical properties were estimated at a strain rate of 200 mm/min using dumbbell-shaped samples (gauge length 25 mm, thickness 2 mm). Mechanical properties, such as tensile moduli, fracture strains, and reinforcing factors, were estimated from tensile test results.

2.4.9. Compressive fatigue and cyclic testing of RTV-SR/CRGO nanocomposites

Compressive mechanical cyclic tests were performed using the universal testing machine. Cyclic testing was performed on cylindrical samples (20 mm diameter and 10 mm thickness) at a strain of 30% for one set of samples and at strains of 10, 30, and 50% for a second set. Multi-hysteresis testing was performed over 500 cycles at a strain of 30% for 1 and 2 phr CRGO in RTV-SR composites (RTV-SR/CRGO (1 and 2 phr, respectively)).

2.4.10. Hardness of RTV-SR/CRGO nanocomposite

The hardness of RTV-SR/CRGO nanocomposites was estimated manually using a Westop durometer as described in ASTM D 2583. Shore A hardness provides a rapid, accurate means of measuring the hardness of the RTV-SR/CRGO nanocomposite. The hardness tests were performed for three samples per specimen, and their median values along with error bars were reported.

2.4.11. Electrochemical conductivity properties

In the frequency range of 0.01–100 kHz, electrochemical impedance spectroscopy (EIS) was used to investigate the electrical conductive activity of the produced electrodes.

2.4.12. Piezoelectric energy harvesting using RTV-SR/CRGO nanocomposites

Mechanical energy harvested by RTV-SR/CRGO nanocomposites was estimated using a cyclic testing machine (Samick-THK, South Korea). Voltage output obtained during the cyclic loading on the flexible energy harvester was measured using a Digital Multimeter (Agilent 34401A, USA). Samples were composed of an elastomer slab of 2 mm thick RTV-SR and a 2 mm RTV-SR/CRGO (1 phr) laminate. The electrodes were composed of 2 phr CNT sandwiched between the elastomer slabs. Cyclic loading was conducted by bi-axial compressive loading at 2 Hz. 1 cm depth of load is applied during the cyclic loading. The optical setup, electrode dimensions and arrangement of electrode and substrate are detailed in the previous study [26].

3. Result and discussions

3.1. FESEM microscopy and CRGO powder purity and morphology

The surface morphology and elemental composition of the CRGO flake were estimated by FESEM (Figure 2). CRGO exhibited an anisotropic, sheet-like morphology. Basically, CRGO consists of stacked graphene layers ranging from 1 to 5 graphene sheets. As previously reported, the properties of RTV-SR/CRGO composites depend on the amount of graphene stacking in CRGO. In addition, the aspect ratio distribution of CRGO flakes also plays an important role in determining the properties of composites. CRGO flakes with a higher aspect ratio provide better reinforcement and also help achieve filler percolation thresholds at lower loadings. In addition, CRGO purity affects the properties (especially mechanical properties) of composites [27]. Elemental mapping of CRGO flakes was performed to determine the distributions of functional species on specimen surfaces and showed carbon and oxygen-containing functional groups were densely distributed on surfaces, though most functional groups were located at the edges of

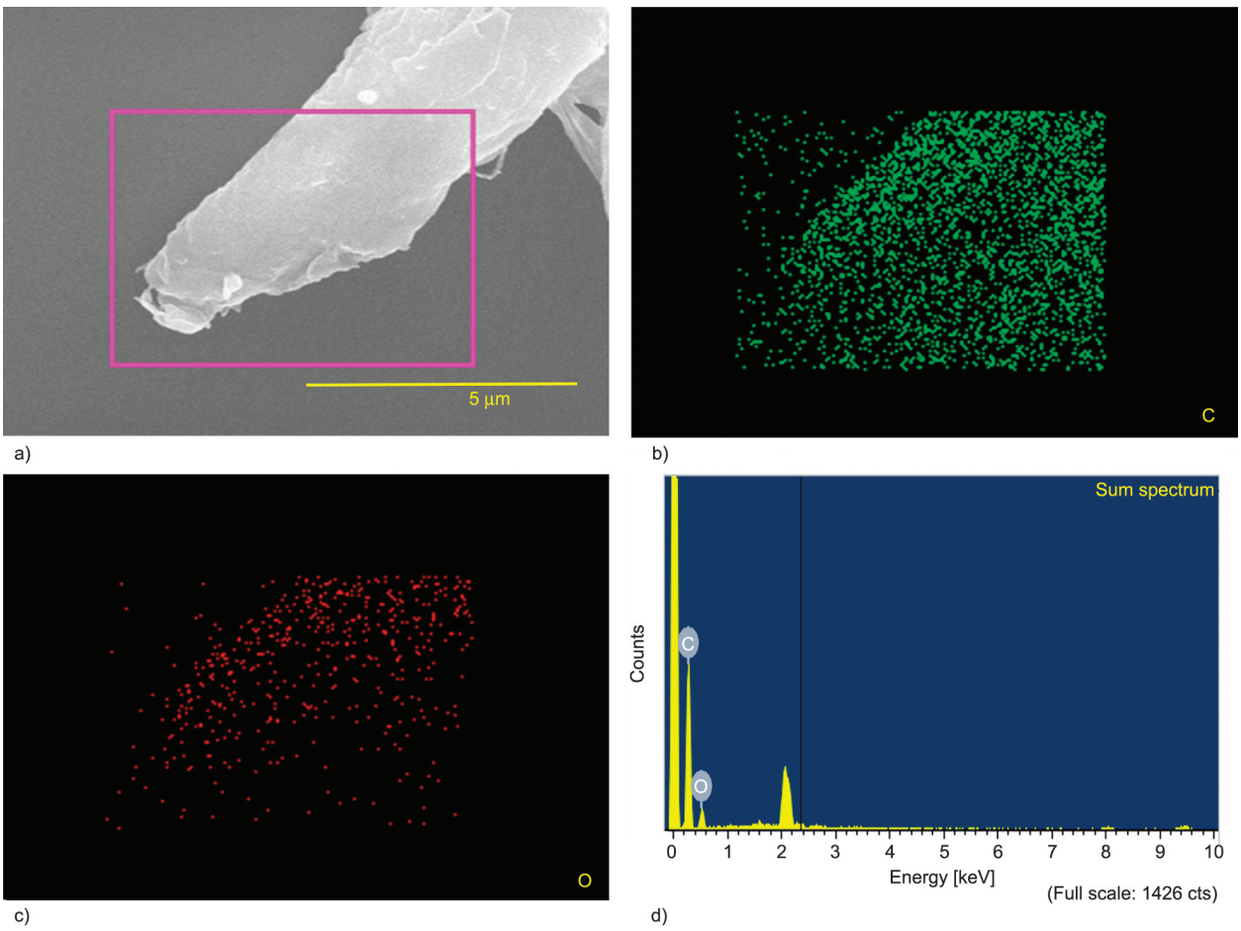

Figure 2. Representative FESEM and EDX images of CRGO flake. (a) SEM micrograph of CRGO; (b-c) Elemental mapping of CRGO; (d) EDX of CRGO.

specimens. SEM-EDX showed CRGO contained 72.6 wt% of carbon and 27.4 wt% of oxygen, which indicated the presence of carbon and oxygen-containing functional groups.

3.2. TEM micrographs of CRGO

CRGO surface morphology was further investigated by TEM (Figure 3). Greater CRGO flake thickness (dark area) indicates more graphene stacking [28].

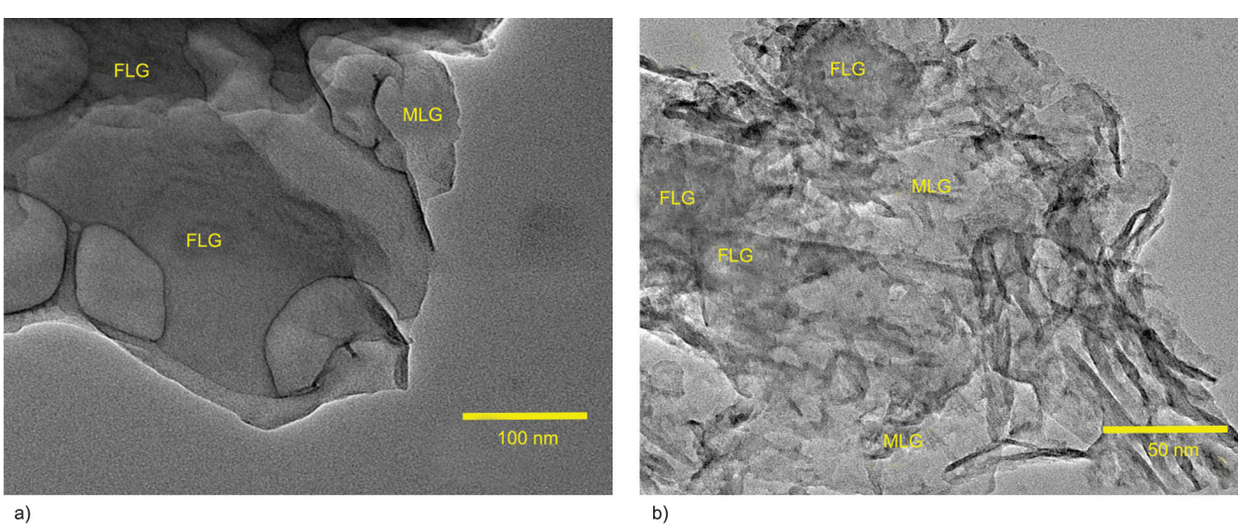

Figure 3. TEM images of CRGO powder: (a) low-resolution image; (b) high-resolution image; MLG indicates monolayer graphene and FLG few-layered graphene.

Thinner flakes (light and transparent areas) indicate lower or no graphene stacking and higher levels of exfoliation [28]. Most of the flakes of CRGO in the TEM image shown in Figure 3 are transparent, indicating graphene was highly exfoliated during the GO to CRGO reduction [28]. Wrinkling of CRGO sheets was observed at high magnification and was attributed to the chemical reduction of GO [29]. High-resolution images showed graphene flakes had an almost interconnected sheet-like morphology and suggested that wrinkles may have resulted from interactions between Van der Waals forces generated in adjacent films. Furthermore, wrinkle formation in CRGO might buffer mechanical properties [30].

3.3. XRD analysis and Raman spectra of CRGO powder

XRD was used to determine the crystal structure of the CRGO flake (Figure 4a). A broad (002) peak was observed in the XRD pattern of CRGO [25], which provides information about stacking thickness [31]. D-spacing between adjacent layers in CRGO can be estimated using Bragg's law, and $D_{hk\ell}$ correlation lengths using Scherrer's equation. By estimating $D_{hk\ell}$ and the interlayer distance between adjacent graphene layers in CRGO, which ranged from 0.4 to 0.44 nm, the number of layers could be estimated. A small diffraction peak at 2θ of near 43.7° is related to the (102) *hkl* plane of the RGO structure and is in agreement with the literature [25]. We found that CRGO flakes were 3–5 graphene layers thick, which agreed with TEM results (Figure 3).

The Raman spectra of carbon nanomaterials such as CRGO generally display three major bands (the D, G, and 2D bands) at different Raman shifts (Figure 4b). The Raman spectrum of CRGO displayed all three characteristic bands (D-band at 1352 cm^{-1}, G-band at 1585 cm^{-1}, and 2D-band at 2730 cm^{-1}). Low-intensity bands such as D+G and 2G were also observed. The Raman spectrum of the CRGO flake showed two different phonon oscillations in the G and 2D bands. The 2D band is extremely sensitive to changes in the structure of the electronic band due to interlayer interactions in CRGO. The D-band indicates the presence of defects in flakes, and its intensity is related to the amount of disorder present. The Raman spectrum of CRGO contained a weak D-band (due to sp^3 hybridized carbon atoms that form few defects) and a strong G-band (due to sp^2 hybridized carbon). For monolayer graphene, the 2D peak is symmetrical and sharp but loses its symmetry when the number of graphene layers increases to five [31].

3.4. XPS and FTIR of CRGO powder

The XPS spectrum of CRGO is presented in Figure 5a and shows a high atomic C/O ratio of 2.04. In Figure 5b, which shows XPS C1s spectra, the energy scale was calibrated internally by setting the binding energy of C=C to 284.67 eV [32]. Deconvolution helped identify four types of carbon [33]. The relative intensities of resolved components showed that as chemical reduction progressed, sp^2 carbons increased and oxygen-containing functional groups decreased. In addition, C–O was also detected at 286.32 eV, and carbonyl O–C=O was detected as a shoulder peak at 289.0 eV [34]. XPS spectra of O1s contained peaks at 531.81 and 533.11 eV, which were assigned to C–O and C=O, respectively (Figure 5c).

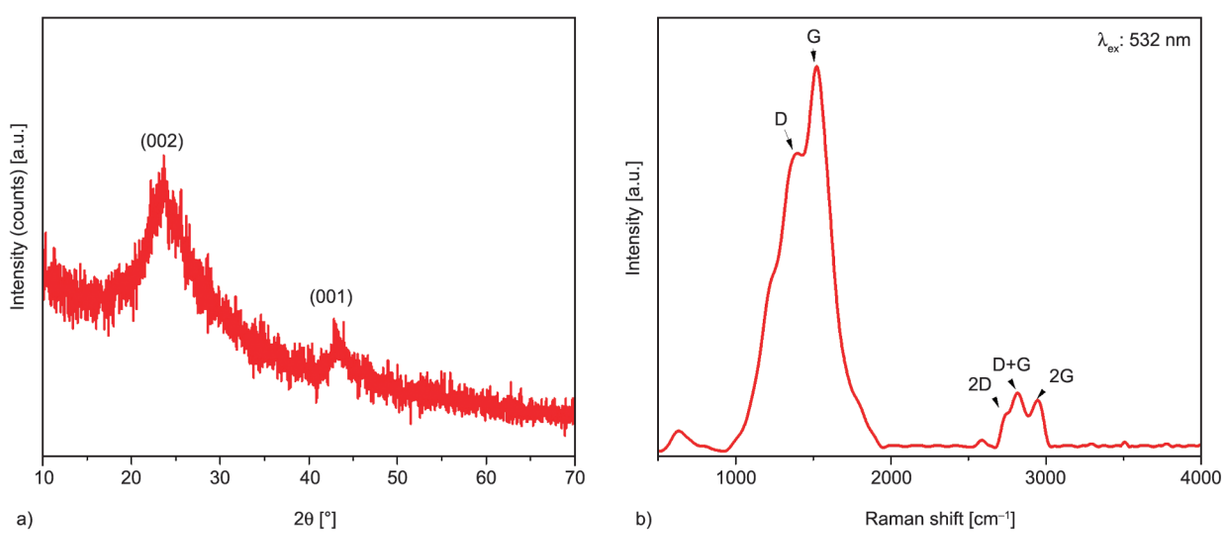

Figure 4. (a) XRD of CRGO; (b) Raman spectrum of CRGO.

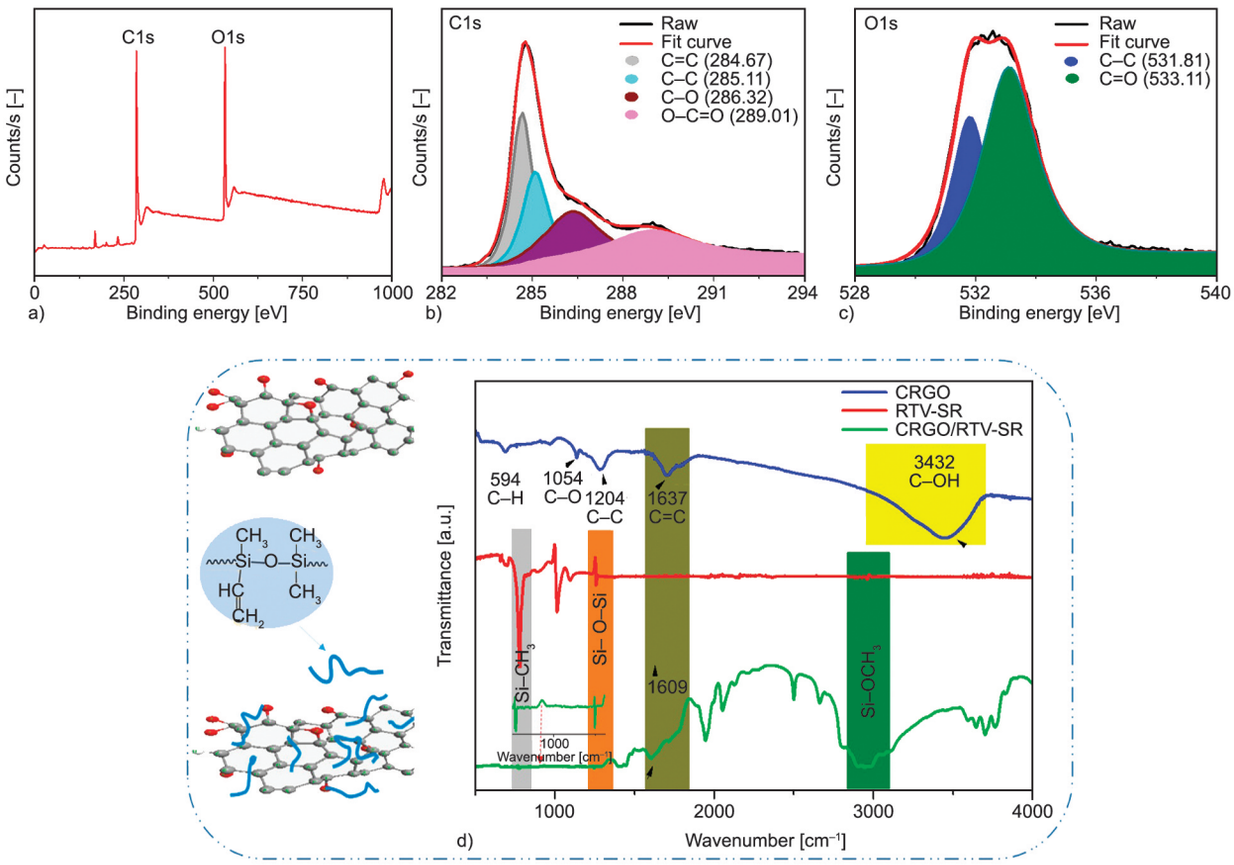

Figure 5. (a) XPS of CRGO, (b, c) high-resolution XPS of CRGO; (d) FTIR of CRGO, RTV-SR, and RTV-SR/CRGO composites.

Fourier transform infrared spectroscopy (FTIR) is a versatile and valuable technique that provides information about the presence of various functional groups. The FTIR spectra of CRGO, RTV-SR, and RTV-SR/CRGO composites are shown in Figure 5d. The IR spectrum of CRGO contained characteristic bands at ~594 cm^{-1}, which were attributed to C–H vibrations, peaks at 1054 and 1204 cm^{-1} attributed to epoxide C–O stretch, and a peak at 1637 cm^{-1} due to skeletal vibrations of C=C aromatic non-oxidized graphitic domains, and thus, confirmed the sp^2 structure of CRGO [35].

In addition, O–H stretch was observed at 3432 cm^{-1}. A comparison of the FTIR spectra of CRGO/RTV-SR and RTV-SR revealed Si-CH_3 stretch at 700–900 cm^{-1} and peaks corresponding to Si–O–Si at 1000–1054 cm^{-1} and C–OCH at 2432 to 3479 cm^{-1} in both samples. [36, 37] However, the intensity of the modified amplitude vibration in the spectrum of CRGO/RTV-SR was greater than in that of RTV-SR, which suggested the C=C bond for sp^2 hybridization of CRGO is significantly grafted into the RTV-SR. The wide of different color rectangles denoted the stretch vibrations range at cm^{-1}.

3.5. CRGO dispersion in RTV-SR/CRGO nanocomposites through optical microscopy

Figure 6a–6c shows that the addition of CRGO to RTV-SR resulted in CRGO network formation at 0.5 phr and long-range network formation at a CRGO loading of 1 phr (shown by the yellow dashed lines). A further increase to 2 phr CRGO (Figure 6d) resulted in the formation of filler-rich zones (yellow circles), and this leads to the formation of efficient filler networks and enhances the electrical properties. The brighter domains of the filler particles can be witnessed in the RTV-SR matrix with the formation of filler percolation threshold between 0.5 to 1 phr CRGO. These brighter domains of filler particles can be easily identified as a homogenous distribution, while filler-rich zones were witnessed at 2 phr CRGO as described in Figure 6d. The very few aggregates in filler-rich zones in CRGO at and after 2 phr could

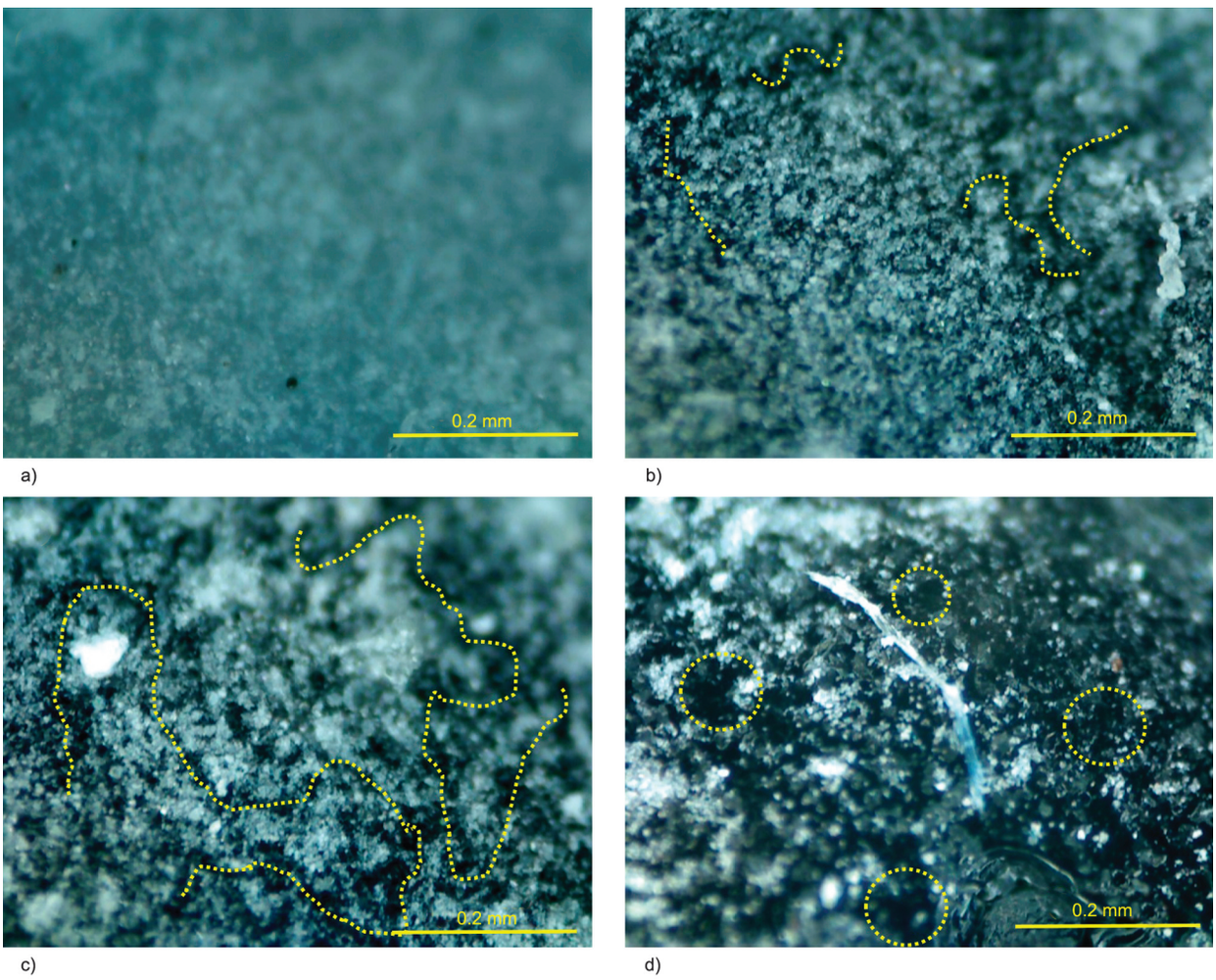

Figure 6. Optical micrographs of (a) RTV-SR; (b) 0.5 phr CRGO; (c) 1 phr CRGO; (d) 2 phr CRGO; (b, c) yellow dashed lines show CRGO network formation in RTV-SR; (d) yellow circles show CRGO aggregation and filler rich zones.

be due to restacking of graphene layers in the CRGO flake owing to Van der Waals interactions between adjacent graphene sheets stacked in the CRGO flake [38]. However, the restacking frequency is lower than pristine GNP due to the higher inter-layer distance in CRGO (0.4–0.44 nm) than GNP flake (0.35 nm) used in preparing CRGO.

The 1 phr CRGO filled RTV-SR where the long-range filler networks are formed, further investigated in-depth via cross-linking density calculations as described in Table 3.

Table 3. Thermodynamic parameters and crosslink density.

Sample	ΔG [J/mol]	ΔS [$\cdot 10^2$ J/mol]	Crosslink density [$\cdot 10^4$ mol/cm^3]
RTV-unfilled	–68.04	22.83	4.76
RTV-0.5 CRGO	–69.04	23.17	4.64
RTV-1.0 CRGO	–63.52	21.32	4.37
RTV-2.0 CRGO	–11.74	3.94	0.90

From the Table 3, it can be found that ΔG and ΔS are better for 0.5 phr CRGO than unfilled rubber. Up to 1 phr of CRGO in the composites, there is no serious loss of ΔG, ΔS, and cross-link densities. However, at 2 phr filler concentration, the favorable thermodynamic parameters largely reduced might be due to reduced cross-link density. It is believed that at a higher concentration of CRGO, the cross-linking reaction through condensation reaction is highly affected and produces a reduced number of cross-links. Since lower ΔG and higher ΔS value indicate better cross-links and higher filler-polymer interactions [22], the CRGO filler is not to be used for more than 1 phr to get balanced properties. After 1 phr CRGO, the polarities of CRGO filler due to oxygen-containing functional groups retards the condensation cross-linking without improving filler-polymer interactions and provide lower mechanical properties to the rubber composite.

3.6. Mechanical properties of RTV-SR/CRGO nanocomposites

Here, we studied the effect of CRGO as a reinforcing filler in RTV-SR and measured the compressive moduli, tensile moduli, fracture strains, and tensile strengths of composites.

3.6.1. Under static compressive strain

Compressive stress-strain curves and moduli at different CRGO loadings in RTV-SR were measured (Figure 8). Compressive stress-strain curves showed that compressive stress increased with compressive modulus, presumably due to increased CRGO and polymer chain packing. Notably, the overall mechanical strength of RTV-SR/CRGO (0.5 phr) was much lower than that of RTV-SR, which we suppose was caused by the functionalization of the CRGO surface, and which suggested that functionalization enhances interfacial interactions (Figure 7) [39]. On the other hand, the introduction of functional groups to the robust sp^2 structure of pristine GNP induced sp^3 bond formation and reduced the reinforcing effect of the CRGO flake.

In addition, the predicted mechanical properties of all three RTV-SR/CRGO nanocomposites approximated to idealized dispersion models, and this is, to some extent, not true in the case of pristine GNP as these nanoplatelets show a higher tendency to agglomerate in the matrix [40]. The method for improving filler dispersion is by improving polymer-filler compatibility or improving interfacial interaction by introducing functionalized groups on the

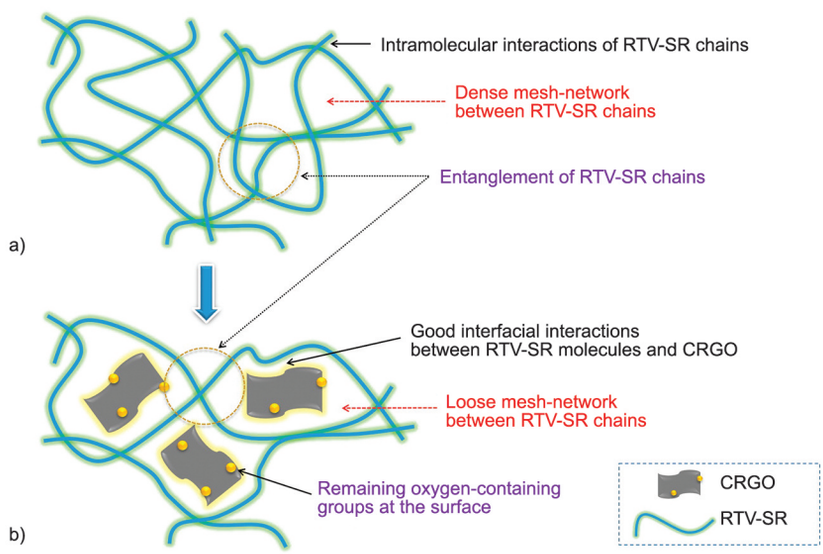

Figure 7. (a) Mechanism of intermolecular interactions in RTV-SR; (b) interfacial interactions between CRGO and RTV-SR at 1 phr.

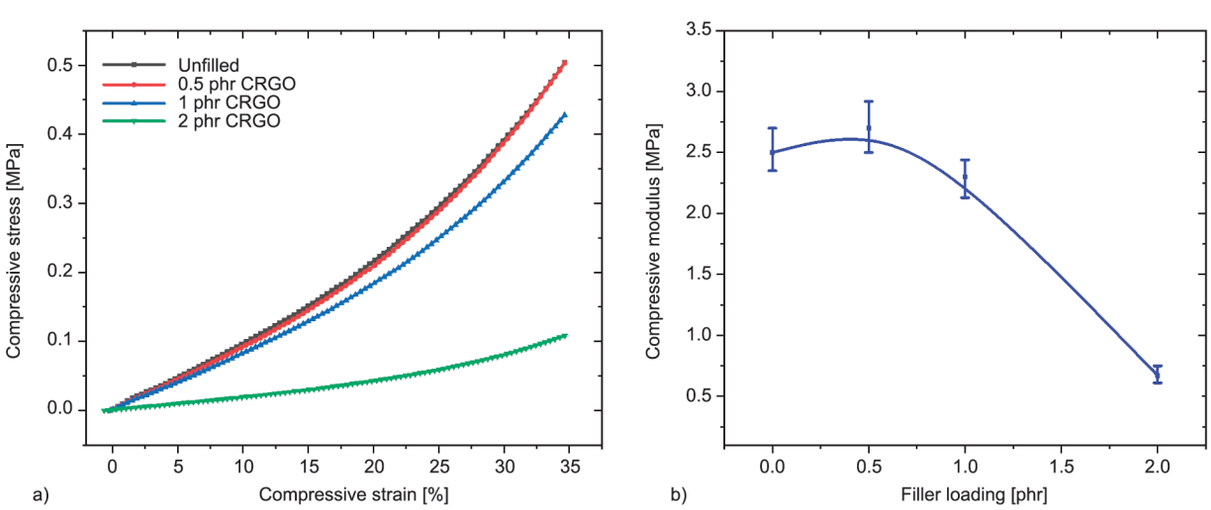

Figure 8. Compressive properties of RTV-SR/CRGO composites; (a) compressive stress-strain curves at the different CRGO loadings; (b) plot showing compressive modulus as a function of CRGO content.

filler's surface, such as CRGO in the present work. However, the sharp fall in compressive modulus, especially for RTV-SR/CRGO (2 phr), was probably due to the restacking of graphene layers in CRGO flake and reduced cross-linking density. The presence of filler-rich zones of graphene in the RTV-SR matrix despite good filler-polymer interactions is supported by the optical micrographs shown in Figure 6d, and is attributed to π–π interactions between adjacent graphene sheets [41].

3.6.2. Mechanical tests under cyclic compressive strain

Cyclic compressive mechanical tests were conducted on RTV-SR/CRGO samples containing different CRGO contents (Figure 9a) at 30% strain and different strain rates (Figure 9b). Compressive load increased when strain increased from 0 to 30% for all three CRGO/RTV-SR composites and returned to its initial state after the stress was released. The increase in load observed upon increasing strain was attributed to increased network densities and packing fractions of CRGO/RTV-SR. For RTV-SR/CRGO composites, when the compressive strain was increased, compressive load also increased, apparently because of enhanced filler network formation. For the investigation of the behaviors of composites under cyclic testing, compressive strain cycles were repeated 500 times. The load was lower for RTV-SR/CRGO (0.5 phr) than for (2 phr) (Figure 9a), but behavior under cyclic strain remained the same. This reduction in compressive load was attributed to the diluting effect of CRGO. RTV-SR/CRGO (2 phr) exhibited the lowest compressive load at all cycles. Interestingly, dissipation losses also reduced on increasing CRGO content, which is believed to have been caused by stress transfer from polymer chains to CRGO in filler-rich zones and an equilibrium between the formation and cleavage of Si–O–Si bonds during cycling. This phenomenon was more evident by multi-hysteresis testing (Figures 9c and 9d). Similarly, as the compressive strain increased from 10%

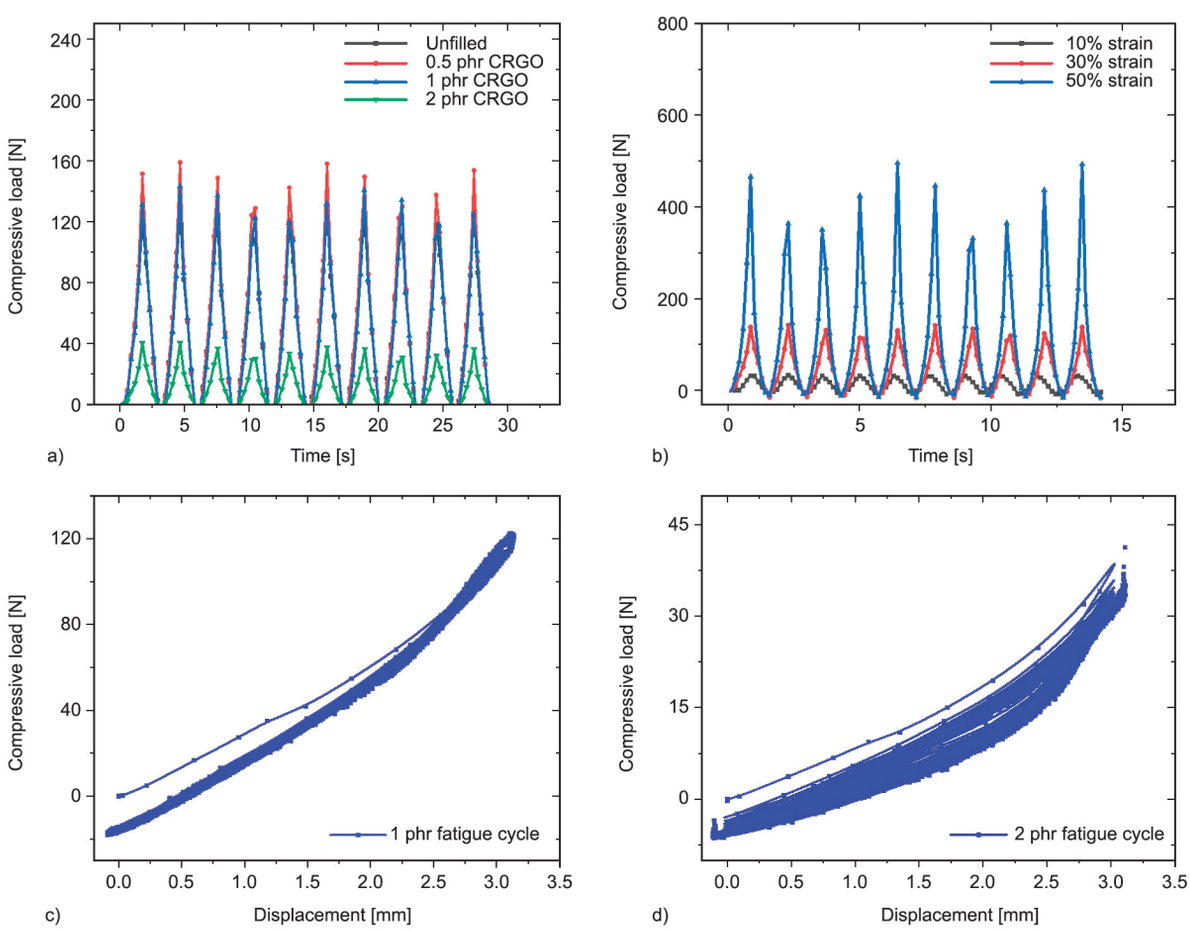

Figure 9. Cyclic compressive mechanical properties; (a) cyclic compressive loads at 30% strain of the RTV-SR/CRGO composites; (b) compressive cyclic loads at different strains for RTV-SR/CRGO (1 phr); (c and d) fatigue cycle outputs for RTV-SR/CRGO (1 phr) and (2 phr) at 30% strain.

to 50% (Figure 9b), compressive load increased markedly and increased dissipation losses [42]. It is noteworthy that RTV-SR composites exhibited greater heat dissipation at a compressive strain of 50% than at 10%. This increase in dissipation losses at higher compressive strain is presumed to have been due to increase bond breakage at higher strain. Thus, it appears that large numbers of bond breakages in RTV-SR/CRGO composites increased dissipation losses and lowered stress transfer from polymer chains to CRGO-rich zones despite the good interfacial interactions induced by CRGO functional groups [42].

Cyclic fatigue testing was conducted on RTV-SR/CRGO (1 phr) and (2 phr) (Figures 9c and 9d) at 30% compressive strain. Both showed dissipation losses and irreversible losses beyond their elastic limits under cyclic loading. Fatigue testing showed that dissipation losses decreased significantly at 30% compressive strain as CRGO content increased from 1 to 2 phr. For both composites, hysteresis loops broadened and recovery to the initial state took longer at the number of cycles increased. This was probably due to plastic deformation in composites, which means that bond breakage and formation rates were not in equilibrium when stress was removed. Furthermore, first cycles exhibited higher dissipation losses than subsequent cycles, perhaps because, during initial cycles, fresh bonds break and then stabilize (new bonds are produced during subsequent cycles). Stress-strain hysteresis might be related to filler network formation, a reduction in the effective volume of the SR, and surface energy distribution on filler surfaces (active regions). Another reason for high energy dissipation might be the release of bound rubber due to the disruption of filler networks when cyclic sweeps are extended to higher strains. In a previous study, it was shown filler clusters could break and become softer under stress and reduce strain amplification factors [43].

3.6.3. Mechanical properties under static tensile strain

True stress-strain curves are presented in Figure 10a, which shows that tensile stress increased with tensile strain until fracture. This increase in tensile stress was attributed to (a) efficient stress transfer from RTV-SR polymer chains to CRGO particles due to good interfacial interaction, and (b) orientations of polymer chains and filler particles in the direction to applied stress that opposed stretching of the composite under strain. On the other hand, tensile modulus (Figure 10) and tensile strength (Figure 10d) fell on increasing CRGO loading, which concurs with the results of a previous study, in which mechanical strength fell on adding CRGO to a polymer matrix [44]. There are several potential causes of this fall in mechanical properties, but it is probably due to the diluting effect of CRGO functional groups in the RTV-SR matrix. Observed filler rich zones on increasing CRGO content from 0.5 to 2 phr may interact with the polymer chains of RTV-SR to form CRGO networks, but we observed modulus and tensile strength fell due to the weak natures of these networks, *i.e.*, strong sp^2 bonding in pristine GNP as compared with weak sp^3 bonding in CRGO. In RTV-SR/CRGO (2 phr), which contained abundant networks, restacking of graphene sheets in CRGO took place despite an increase in interlayer thickness (0.4 to 0.44 nm; the interlayer thickness of pristine GNP is 0.33 nm), and this led to reductions in modulus and tensile strength. Another reason for fall in mechanical properties at 2 phr CRGO is due to significant reduction in cross-linking density (Table 3).

On the other hand, fracture strain (Figure 10c) increased with CRGO loading, presumably due to chemical interactions between CRGO functional and the RTV-SR matrix as well as physical adsorption of CRGO particles onto RTV-SR polymer shells. These functional groups in CRGO are carbon and oxygen-based, as demonstrated in Figures 5b and 5c. Another reason for the higher fracture strain observed (especially at 2 phr, which caused a ~100% improvement) might be due to the formation of filler rich zones in the RTV-SR matrix (Figure 6d), which act as solid lubricants due to graphene sheet/graphene sheet slippage under tensile strain and improve fracture strains. Furthermore, our results agree with those of a previous study [45]. Song *et al*. [45] showed that SR has poor tensile strength (0.4 MPa) and fracture strain (115%), but that the addition of a filler, in single or hybrid form, can improve mechanical properties dramatically especially fracture strain.

3.7. Hardness of the RTV-SR/CRGO nanocomposites

The hardness of composites importantly determines various mechanical properties, especially stiffness, and depends on a number of factors such as the modulus of the virgin polymer, filler reinforcement, filler networking, and viscoelasticity. In particular,

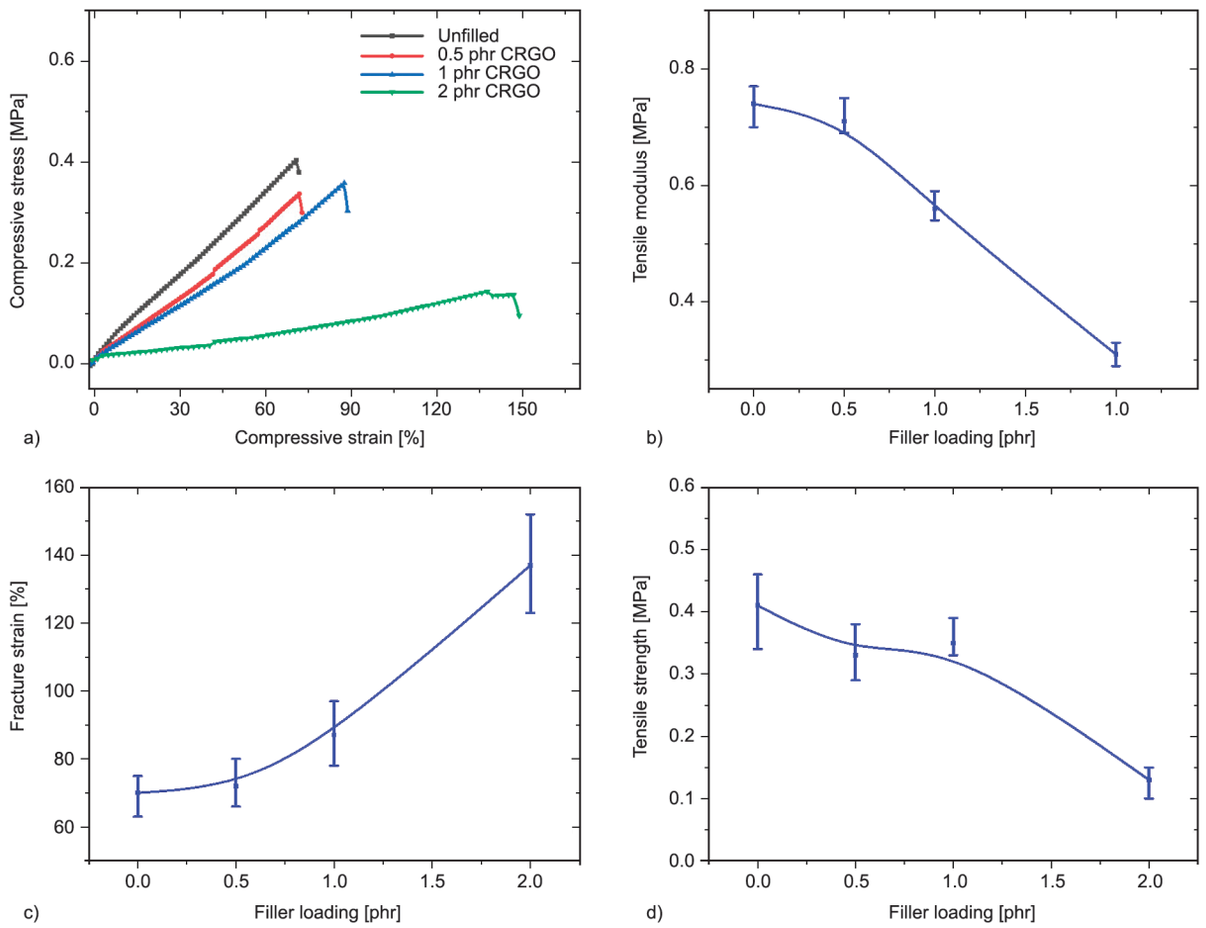

Figure 10. Tensile mechanical properties; (a) tensile stress profiles as a function of tensile strain; (b) tensile modulus (c) fracture strain, and (d) tensile strength as functions of CRGO loadings in RTV-SR composites.

micro-hardness and its distribution in a composite are important since high micro-hardness is sufficient enough to break water films on the rubber surface. However, the hardness is mostly affected by the high elasticity of polymer matrices such as the RTV-SR matrix. In order to study how soft rubber produce scratches on a glassy surface, the hardness of the filler was taken into account [46]. Shore A hardness of the three RTV-SR/CRGO composites was investigated (Figure 11). Hardness remained stable until a CRGO loading of 1 phr was reached but then fell sharply at a loading of 2 phr. This behavior indicated that CRGO had a diluent effect (Figure 6d), and the formation of filler-rich zones in the RTV-SR matrix. Another reason for the fall in hardness at 2 phr CRGO is the significant reduction in cross-linking density (Table 3). The gradual decline of hardness shown in Figure 11 implies that some kind of permanent softness or dilution by CRGO occurred in RTV-SR/CRGO composites. RTV-SR/CRGO (2 phr) remained soft for more than one month at room temperature without any significant change in hardness. This property of permanent softness, even without the use of a thinner or additional diluent, is promising for industrial applications such as soft actuators. A number of mechanisms may be responsible for lowering the stiffness of RTV-SR/CRGO composites containing ≥2 phr of CRGO, though increased CRGO filler-rich zones

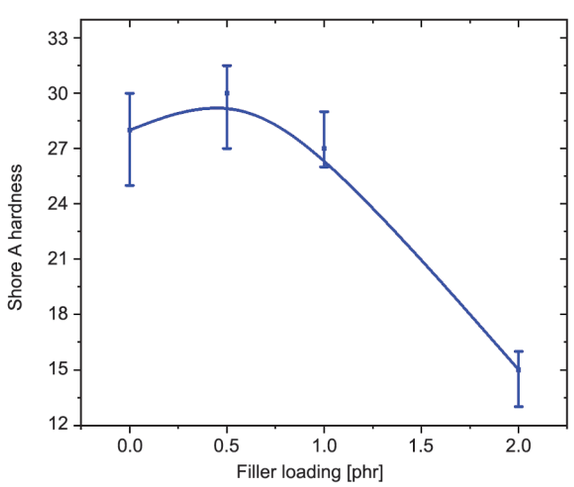

Figure 11. Hardness of composites containing different concentrations of CRGO.

probably provide the best explanation. It is well known that rubber composites with a Shore A hardness of <65 are softer than glass [46]. The composites used in this study may be useful for soft robotics and other industrial applications such as energy harvesting (Figure 14).

3.8. Reinforcing factor and reinforcing efficiency

The filler networks were studied by reinforcing factors and reinforcing the efficiency of the filler (Figure 12). Generally, the reinforcing factor below one is termed a poor reinforcing effect of the filler and is related to poor filler networks and related lower cross-linking density. The reinforcing efficiency at 70% strain for tensile strain and 30% for the compressive strain was studied. At this strain, there is a dominance of filler networks and is related to filler reinforcement. The negative reinforcing efficiency further insight poor reinforcement by fillers and also related to poor cross-linking density by curatives. Filler networking was further studied through electrical conductivity measurements shown in Figure 13.

3.9. Electrochemical conductivity properties

The EIS spectra of the electrodes, as well as an *R* (*CR*) *W* equivalent circuit, are shown in Figure 13. Series resistance/solution resistance is defined as the initial crossing of the EIS spectrum on the X-axis (real impedance) in high frequency (R_s). All of the electrodes have a solution resistance of 0.50 ohms. At higher frequencies, the diameter of the displayed

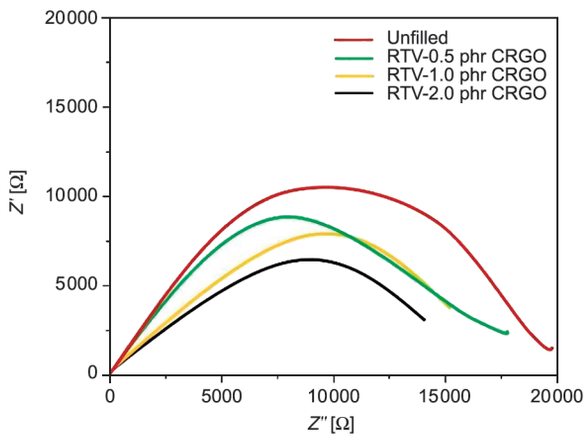

Figure 13. Electrochemical conductivity of composites containing different types of CRGO composites.

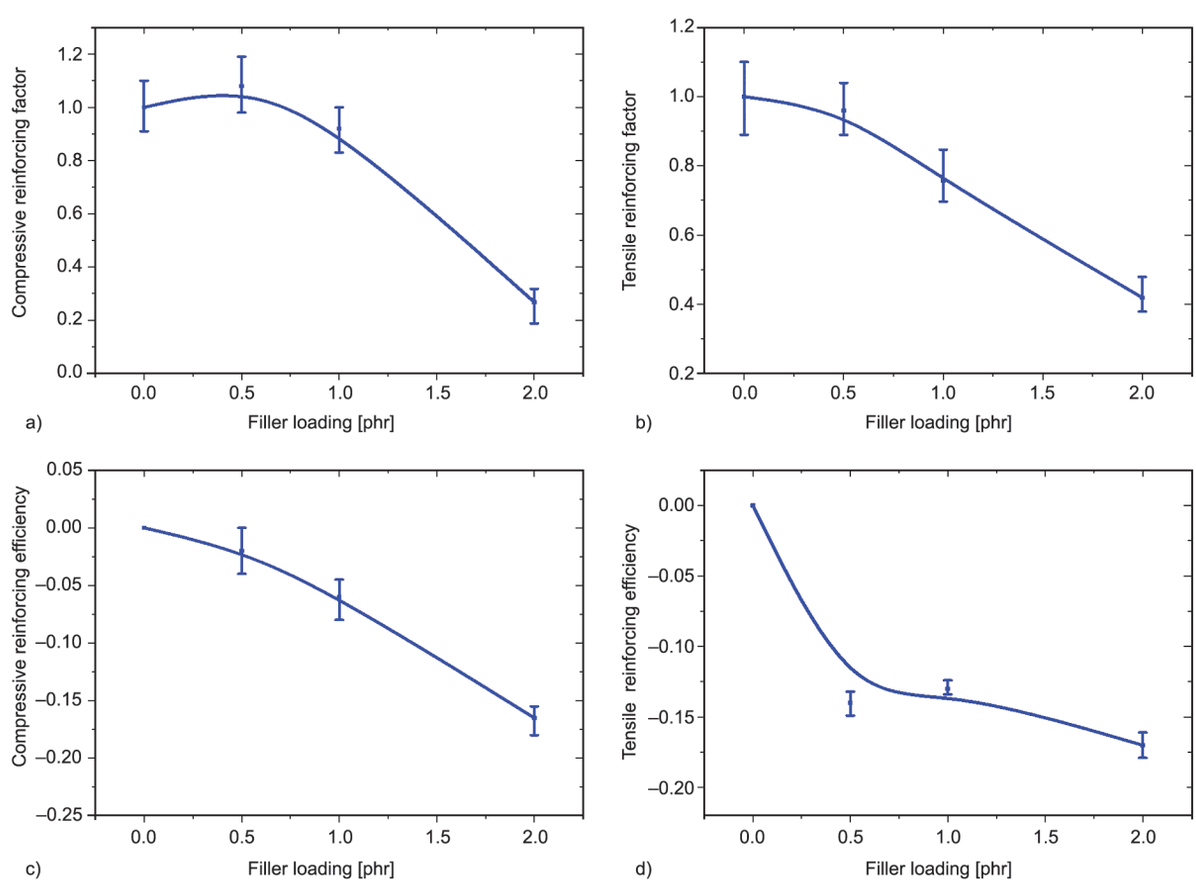

Figure 12. Reinforcing factor (a) compressive and (b) tensile; reinforcing efficiency (c) compressive and (d) tensile at different concentrations of CRGO.

semicircle represents the electrodes' charge transfer resistance (R_{ct}). Unfilled RTV, 0.5, 1, and 2 phr CRGO filled RTV composite electrodes had R_{ct} values of 20, 17.8, 16.5, and 15 Ω, respectively. Hence, the electrical conductivity measurements shows that the electrical resistance decrease as the concentration of CRGO increase in RV-SR and thus can be hypothesized the formation of efficient filler networks of CRGO in the rubber matrix.

4. Applications

4.1. Piezoelectric energy harvesting using RTV-SR/CRGO nanocomposites

Flexible devices produce voltage directly when exposed to mechanical strain. The generation of small amounts of electricity using flexible energy composite harvesters (sufficient to drive low consumption devices such as LEDs) is key to meeting increasing energy demands. Large amounts of energy could be generated by simple mechanical motion, such as walking, without affecting the environment, and thus, these eco-friendly devices have attracted the attention of scientists. Figure 14 shows the output of RTV-SR/CRGO (1 phr) exposed to bi-axial strain. Energy generation was stable for an RTV-SR elastomer slab (Figure 14a) but increased with cycle number for an RTV-SR/CRGO (1 phr) slab (Figure 14b). The behaviors of different types of elastomer slabs were attributed to their chemistries. The elastomer slab based on RTV-SR behaved as a stable dielectric rubber, whereas the RTV-SR/ CRGO (1 phr) slab stabilized after a few cycles and generated more energy as cycle numbers increased. Carbon and oxygen-containing functional groups on CRGO improved interfacial interactions but reduced dielectric rubber properties. Increases in voltage on increasing cycle numbers of cycles have been shown to be caused by the activations of charge carriers by cycle numbers in elastomer slabs based on RTV-SR/CRGO composites [47].

5. Conclusions

RTV-SR/CRGO composites were prepared by solution casting and characterized for mechanical properties and subsequently for energy harvesting. CRGO was prepared by oxidizing GNP and subsequent chemical reduction to form CRGO. TEM and XRD showed CRGO was composed of 1 to 5 layered graphene. Static tensile testing and compressive mechanical measurements showed that the modulus of RTV-SR decreased on increasing CRGO loading and that it fell significantly at a CRGO loading of 2 phr, at which softness was increased and stiffness decreased. We found that as little as 2 phr CRGO in RTV-SR transformed the normally rigid RTV-SR into a soft composite with a hardness decrease to 15. In addition, the compressive modulus decreased to 0.6 MPa. However, it is good that the dissipation losses decrease at 2 phr CRGO, which is good for industrial applications. For tensile mechanical properties, the fracture strain increases to 100% while tensile strength falls strongly to 0.1 MPa. Moreover, the composites at 2 phr of CRGO exhibited permanent softness. During cyclic compressive fatigue testing, first cycles exhibited higher heat dissipation losses, and subsequent cycles led to plastic deformation of composites. However, RTV-SR/CRGO (2 phr) showed

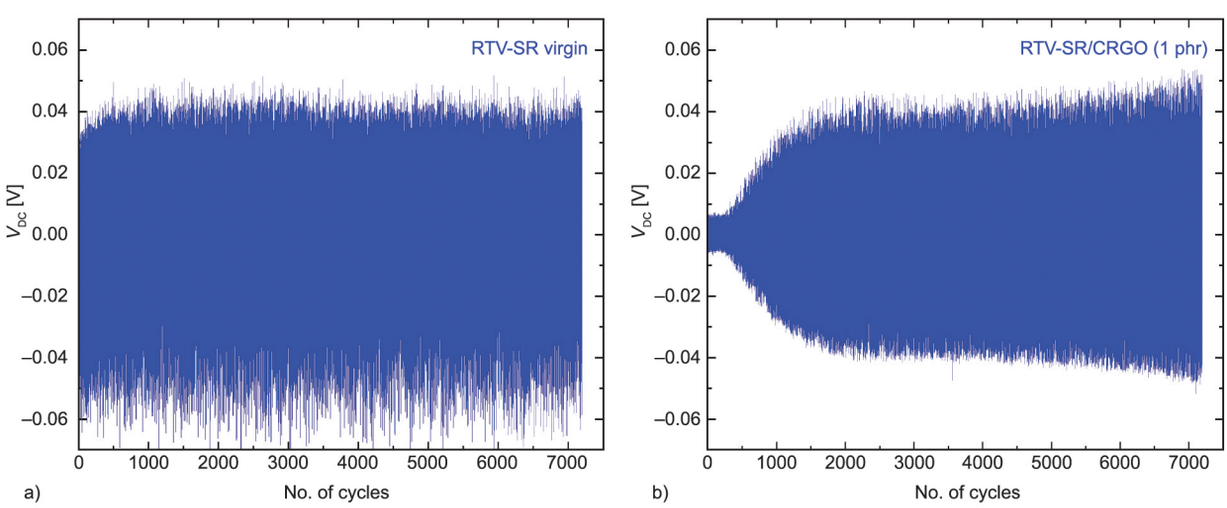

Figure 14. Energy harvesting of RTV-SR composites (a) output voltages for RV-SR; (b) output voltages for RTV-SR/CRGO (1 phr).

significant plastic deformation and reductions in heat dissipation losses. Moreover, this work demonstrates the formation of efficient filler networks of CRGO through improved electrochemical properties. In addition, a decrease in cross-linking density leads to the formation of mechanically soft composites with high fracture strain which are suitable for soft applications. Besides this, this work attaches to the readers a possible correlation between mechanical properties with a change in cross-linking density and the pH of CRGO. These properties were helpful in obtaining high voltage via a piezoelectric energy harvesting device. Energy harvesting experiments showed that RTV-SR generated a stable output voltage but that output voltages increased with cycle number for RTV-SR/CRGO composites.

Acknowledgements

The research work was supported by the NRF fund of the Korean Ministry of Education (Grant No. 2017R1D1A3B03031732).
Vineet Kumar and Tapas Kumar Mandal contribute equally to the work.

References

[1] Li H., Liang Y., Gao G., Wei S., Jian Y., Le X., Lu W., Liu Q., Zhang J., Chen T.: Asymmetric bilayer CNTs-elastomer/hydrogel composite as soft actuators with sensing performance. Chemical Engineering Journal, **415**, 128988 (2021). https://doi.org/10.1016/j.cej.2021.128988

[2] Hu Y., Zhou C., Wang H., Chen M., Zeng G., Liu Z., Liu Y., Wang W., Wu T., Shao B., Liang Q.: Recent advance of graphene/semiconductor composite nanocatalysts: Synthesis, mechanism, applications and perspectives. Chemical Engineering Journal, **414**, 128795 (2021). https://doi.org/10.1016/j.cej.2021.128795

[3] Luheng W., Tianhuai D., Peng W.: Influence of carbon black concentration on piezoresistivity for carbon-black-filled silicone rubber composite. Carbon, **47**, 3151–3157 (2009). https://doi.org/10.1016/j.carbon.2009.06.050

[4] Martins P. A. L. S., Natal Jorge R. M., Ferreira A. J. M.: A comparative study of several material models for prediction of hyperelastic properties: Application to silicone-rubber and soft tissues. Strain, **42**, 135–147 (2006). https://doi.org/10.1111/j.1475-1305.2006.00257.x

[5] Song J., Peng Z., Zhang Y.: Enhancement of thermal conductivity and mechanical properties of silicone rubber composites by using acrylate grafted siloxane copolymers. Chemical Engineering Journal, **391**, 123476 (2020). https://doi.org/10.1016/j.cej.2019.123476

[6] Kumar V., Lee D-J.: Studies of nanocomposites based on carbon nanomaterials and RTV silicone rubber. Journal of Applied Polymer Science, **134**, 44407 (2017). https://doi.org/10.1002/app.44407

[7] Zhao C., Wang J., Zhao B., Chang E., Lee P. C., Park C. B.: Electrically percolated nanofibrillar composites with core-sheath structures from completely wet ternary polymer blends. Chemical Engineering Journal, **419**, 129603 (2021). https://doi.org/10.1016/j.cej.2021.129603

[8] Gong L-X., Pei Y-B., Han Q-Y., Zhao L., Wu L-B., Jiang J-X., Tang L-C.: Polymer grafted reduced graphene oxide sheets for improving stress transfer in polymer composites. Composites Science and Technology, **134**, 144–152 (2016). https://doi.org/10.1016/j.compscitech.2016.08.014

[9] Wang X., Gong L-X., Tang L-C., Peng K., Pei Y-B., Zhao L., Wu L-B., Jiang J-X.: Temperature dependence of creep and recovery behaviors of polymer composites filled with chemically reduced graphene oxide. Composites Part A: Applied Science and Manufacturing, **69**, 288–298 (2015). https://doi.org/10.1016/j.compositesa.2014.11.031

[10] Ma R., Zhou Y., Bi H., Yang M., Wang J., Liu Q., Huang F.: Multidimensional graphene structures and beyond: Unique properties, syntheses and applications. Progress in Materials Science, **113**, 100665 (2020). https://doi.org/10.1016/j.pmatsci.2020.100665

[11] Gabris M. A., Ping J.: Carbon nanomaterial-based nanogenerators for harvesting energy from environment. Nano Energy, **90**, 106494 (2021). https://doi.org/10.1016/j.nanoen.2021.106494

[12] Selim M. S., Shenashen M. A., El-Safty S. A., Higazy S. A., Selim M. M., Isago H., Elmarakbi A.: Recent progress in marine foul-release polymeric nanocomposite coatings. Progress in Materials Science, **87**, 1–32 (2017). https://doi.org/10.1016/j.pmatsci.2017.02.001

[13] Selim M. S., El-Safty S. A., Shenashen M. A., Higazy S. A., Elmarakbi A.: Progress in biomimetic leverages for marine antifouling using nanocomposite coatings. Journal of Materials Chemistry B, **8**, 3701–3732 (2020). https://doi.org/10.1039/C9TB02119A

[14] Gong L-X., Zhao L., Tang L-C., Liu H-Y., Mai Y-W.: Balanced electrical, thermal and mechanical properties of epoxy composites filled with chemically reduced graphene oxide and rubber nanoparticles. Composites Science and Technology, **121**, 104–114 (2015). https://doi.org/10.1016/j.compscitech.2015.10.023

[15] Kang J., Kim J., Choi K., Hong P. H., Park H. J., Kim K., Kim Y. K., Moon G., Jeon H., Lee S., Ko M. J., Hong S. W.: A water-triggered highly self-healable elastomer with enhanced mechanical properties achieved using localized zwitterionic assemblies. Chemical Engineering Journal, **420**, 127636 (2021). https://doi.org/10.1016/j.cej.2020.127636

[16] Shit S. C., Shah P.: A review on silicone rubber. National Academy Science Letters, **36**, 355–365 (2013). https://doi.org/10.1007/s40009-013-0150-2

[17] Papageorgiou D. G., Kinloch I. A., Young R. J.: Graphene/elastomer nanocomposites. Carbon, **95**, 460–484 (2015). https://doi.org/10.1016/j.carbon.2015.08.055

[18] Frasca D., Schulze D., Wachtendorf V., Huth C., Schartel B.: Multifunctional multilayer graphene/elastomer nanocomposites. European Polymer Journal, **71**, 99–113 (2015). https://doi.org/10.1016/j.eurpolymj.2015.07.050

[19] Song J., Zhang Y.: Vertically aligned silicon carbide nanowires/reduced graphene oxide networks for enhancing the thermal conductivity of silicone rubber composites. Composites Part A: Applied Science and Manufacturing, **133**, 105873 (2020). https://doi.org/10.1016/j.compositesa.2020.105873

[20] Chen J., Yao B., Li C., Shi G.: An improved Hummers method for eco-friendly synthesis of graphene oxide. Carbon, **64**, 225–229 (2013). https://doi.org/10.1016/j.carbon.2013.07.055

[21] Usuki A., Kojima Y., Kawasumi M., Okada A., Fukushima Y., Kurauchi T., Kamigaito O.: Synthesis of nylon 6-clay hybrid. Journal of Materials Research, **8**, 1179–1184 (1993). https://doi.org/10.1557/JMR.1993.1179

[22] Panampilly B., Thomas S.: Nano ZnO as cure activator and reinforcing filler in natural rubber. Polymer Engineering and Science, **53**, 1337–1346 (2013). https://doi.org/10.1002/pen.23383

[23] Flory P. J., Rehner J.: Statistical mechanics of cross-linked polymer networks II. Swelling. The Journal of Chemical Physics, **11**, 521–526 (1943). https://doi.org/10.1063/1.1723792

[24] Yang X., Li Z., Jiang Z., Wang S., Liu H., Xu X., Wang D., Miao Y., Shang S., Song Z.: Mechanical reinforcement of room-temperature-vulcanized silicone rubber using modified cellulose nanocrystals as cross-linker and nanofiller. Carbohydrate Polymers, **229**, 115509 (2020). https://doi.org/10.1016/j.carbpol.2019.115509

[25] Gupta B., Kumar N., Panda K., Kanan V., Joshi S., Visoly-Fisher I.: Role of oxygen functional groups in reduced graphene oxide for lubrication. Scientific Reports, **7**, 45030 (2017). https://doi.org/10.1038/srep45030

[26] Manikkavel A., Kumar V., Kim J., Lee D. J., Park S. S.: Investigation of high temperature vulcanized and room temperature vulcanized silicone rubber based on flexible piezo-electric energy harvesting applications with multi-walled carbon nanotube reinforced composites. Polymer Composites, **43**, 1305-1318 (2022). https://doi.org/10.1002/pc.26449

[27] Kumar V., Lee D-J.: Effects of purity in single-wall carbon nanotubes into rubber nanocomposites. Chemical Physics Letters, **715**, 195–203 (2019). https://doi.org/10.1016/j.cplett.2018.11.042

[28] Ramya A. V., Mohan A. N., Manoj B.: Wrinkled graphene: Synthesis and characterization of few layer graphene-like nanocarbons from kerosene. Materials Science-Poland, **34**, 330–336 (2016). https://doi.org/10.1515/msp-2016-0061

[29] Yi Z., Qian Y., Jiang S., Li Y., Lin N., Qian Y.: Self-wrinkled graphene as a mechanical buffer: A rational design to boost the K-ion storage performance of Sb_2Se_3 nanoparticles. Chemical Engineering Journal, **379**, 122352 (2020). https://doi.org/10.1016/j.cej.2019.122352

[30] Galimberti M., Kumar V., Coombs M., Cipolletti V., Agnelli S., Pandini S., Conzatti L.: Filler networking of a nanographite with a high shape anisotropy and synergism with carbon black in poly(1,4-cis-isoprene)–based nanocomposites. Rubber Chemistry and Technology, **87**, 197–218 (2014). https://doi.org/10.5254/rct.13.87903

[31] Graf D., Molitor F., Ensslin K., Stampfer C., Jungen A., Hierold C., Wirtz L.: Spatially resolved Raman spectroscopy of single- and few-layer graphene. Nano Letters, **7**, 238–242 (2007). https://doi.org/10.1021/nl061702a

[32] Davis D. W., Shirley D. A.: The prediction of core-level binding-energy shifts from CNDO molecular orbitals. Journal of Electron Spectroscopy and Related Phenomena, **3**, 137–163 (1974). https://doi.org/10.1016/0368-2048(74)80005-8

[33] Ganguly A., Sharma S., Papakonstantinou P., Hamilton J.: Probing the thermal deoxygenation of graphene oxide using high-resolution *in situ* X-ray-based spectroscopies. The Journal of Physical Chemistry C, **115**, 17009–17019 (2011). https://doi.org/10.1021/jp203741y

[34] Gardner S. D., Singamsetty C. S. K., Booth G. L., He G-R., Pittman C. U.: Surface characterization of carbon fibers using angle-resolved XPS and ISS. Carbon, **33**, 587–595 (1995). https://doi.org/10.1016/0008-6223(94)00144-O

[35] Krishnamoorthy K., Kim G-S., Kim S. J.: Graphene nanosheets: Ultrasound assisted synthesis and characterization. Ultrasonics Sonochemistry, **20**, 644–649 (2013). https://doi.org/10.1016/j.ultsonch.2012.09.007

[36] Kumar S., Maiti S. N.: Studies on polycarbonate and polydimethylsiloxane rubber blends. Polymer-Plastics Technology and Engineering, **46**, 427–433 (2007). https://doi.org/10.1080/03602550701244634

[37] Wawrzyn E., Schartel B., Seefeldt H., Karrasch A., Jäger C.: What reacts with what in bisphenol A polycarbonate/silicon rubber/bisphenol A bis(diphenyl phosphate) during pyrolysis and fire behavior? Industrial and Engineering Chemistry Research, **51**, 1244–1255 (2012). https://doi.org/10.1021/ie201908s

[38] Yang X., Zhu J., Qiu L., Li D.: Bioinspired effective prevention of restacking in multilayered graphene films: Towards the next generation of high-performance supercapacitors. Advanced Materials, **23**, 2833–2838 (2011). https://doi.org/10.1002/adma.201100261

[39] Ma P-C., Mo S-Y., Tang B-Z., Kim J-K.: Dispersion, interfacial interaction and re-agglomeration of functionalized carbon nanotubes in epoxy composites. Carbon, **48**, 1824–1834 (2010). https://doi.org/10.1016/j.carbon.2010.01.028

[40] Wajid A. S., Ahmed H. S. T., Das S., Irin F., Jankowski A. F., Green M. J.: High-performance pristine graphene/epoxy composites with enhanced mechanical and electrical properties. Macromolecular Materials and Engineering, **298**, 339–347 (2013). https://doi.org/10.1002/mame.201200043

[41] Li J., Östling M.: Prevention of graphene restacking for performance boost of supercapacitors – A review. Crystals, **3**, 163–190 (2013). https://doi.org/10.3390/cryst3010163

[42] Suhr J., Koratkar N. A.: Energy dissipation in carbon nanotube composites: A review. Journal of Materials Science, **43**, 4370–4382 (2008). https://doi.org/10.1007/s10853-007-2440-x

[43] Govindjee S.: An evaluation of strain amplification concepts *via* monte carlo simulations of an ideal composite. Rubber Chemistry and Technology, **70**, 25–37 (1997). https://doi.org/10.5254/1.3538416

[44] Zhang H., Park J-H., Yoon K-B.: Excellent electrically conductive PE/rGO nanocomposites: *In situ* polymerization using rGO-supported MAO cocatalysts. Composites Science and Technology, **154**, 85–91 (2018). https://doi.org/10.1016/j.compscitech.2017.11.012

[45] Song P., Song J., Zhang Y.: Stretchable conductor based on carbon nanotube/carbon black silicone rubber nanocomposites with highly mechanical, electrical properties and strain sensitivity. Composites Part B: Engineering, **191**, 107979 (2020). https://doi.org/10.1016/j.compositesb.2020.107979

[46] Wang Y-X., Wu Y-P., Li W-J., Zhang L-Q.: Influence of filler type on wet skid resistance of SSBR/BR composites: Effects from roughness and micro-hardness of rubber surface. Applied Surface Science, **257**, 2058–2065 (2011). https://doi.org/10.1016/j.apsusc.2010.08.129

[47] McKay T. G., Rosset S., Anderson I. A., Shea H.: An electroactive polymer energy harvester for wireless sensor networks. Journal of Physics: Conference Series, **476**, 012117 (2013). https://doi.org/10.1088/1742-6596/476/1/012117